Climatology of Surface Meteorology, Surface Fluxes, Cloud Fraction, and Radiative Forcing over the Southeast Pacific from Buoy Observations

VIRENDRA P. GHATE AND BRUCE A. ALBRECHT

Division of Meteorology and Oceanography, University of Miami, Miami, Florida

CHRISTOPHER W. FAIRALL

NOAA/Earth System Research Laboratory/Physical Sciences Division, Boulder, Colorado

ROBERT A. WELLER

Physical Oceanography Department, Woods Hole Oceanographic Institution, Woods Hole, Massachusetts

(Manuscript received 5 December 2008, in final form 15 April 2009)

ABSTRACT

A 5-yr climatology of the meteorology, including boundary layer cloudiness, for the southeast Pacific region is presented using observations from a buoy located at 20°S, 85°W. The sea surface temperature and surface air temperature exhibit a sinusoidal seasonal cycle that is negatively correlated with surface pressure. The relative humidity, wind speed, and wind direction show little seasonal variability. But the advection of cold and dry air from the southeast varies seasonally and is highly correlated with the latent heat flux variations. A simple model was used to estimate the monthly cloud fraction using the observed surface downwelling longwave radiative flux and surface meteorological parameters. The annual cycle of cloud fraction is highly correlated to that of S. A. Klein: lower-tropospheric stability parameter (0.87), latent heat flux (−0.59), and temperature and moisture advection (0.60). The derived cloud fraction compares poorly with the International Satellite Cloud Climatology Project (ISCCP)-derived low-cloud cover but compares well (0.86 correlation) with ISCCP low- plus middle-cloud cover. The monthly averaged diurnal variations in cloud fraction show marked seasonal variability in the amplitude and temporal structure. The mean annual cloud fraction is lower than the mean annual nighttime cloud fraction by about 9%. Annual and diurnal cycles of surface longwave and shortwave cloud radiative forcing were also estimated. The longwave cloud radiative forcing is about 45 W m^{-2} year-round, but, because of highly negative shortwave cloud radiative forcing, the net cloud radiative forcing is always negative with an annual mean of −50 W m^{-2}.

1. Introduction

Marine stratocumulus (Scu) clouds form over eastern subtropical oceans with relatively low sea surface temperature (SST) and beneath a strong temperature inversion (Albrecht et al. 1988). These clouds strongly influence the global radiation budget, since they reflect most of the incoming solar radiation because of their high albedo (compared with the ocean background) but emit longwave radiation at values comparable to the ocean surface (because of low altitude). Hence they have a net cooling effect on the marine atmospheric boundary layer (MABL). Randall et al. (1984) estimated that a 4% increase in the cloud cover of these clouds can compensate global warming because of doubling of CO_2. Using different general circulation models (GCMs), Slingo (1990) found that a relative increase of 15%–20% in the cloud cover is necessary to offset global warming. He argued that the major uncertainty comes from the low-cloud cover and that an accuracy of 1% in absolute terms is required to predict climate change correctly.

Because of their high impact on the earth's radiation budget, it is necessary to represent Scu clouds with fair accuracy in the GCMs. It is believed that the warmer-than-observed SST fields simulated off the west coast of the continents in the subtropical regions in some models

Corresponding author address: Virendra P. Ghate, RSMAS/MPO, University of Miami, 4600 Rickenbacker Causeway, Miami, FL 33149.
E-mail: vghate@rsmas.miami.edu

DOI: 10.1175/2009JCLI2961.1

are due to poor representation of Scu clouds in the atmospheric models (Bretherton et al. 2004). This can lead to positive SST bias of several degrees in coupled GCMs (CGCMs) (e.g., Kiehl and Gent 2004; Wittenberg et al. 2006; Tiexeria et al. 2008; and others). Attempts have been made to develop MABL cloud parameterizations that yield higher Scu cloud cover than that in some current models (e.g., Bachiochi and Krishnamurti 2000).

There have been many observational studies of marine Scu using satellite (Minnis and Harrison 1984; Klein and Hartmann 1993; Rozendaal et al. 1995) and surface-based observations (Norris 1998a,b; Cronin et al. 2006; Bretherton et al. 2004; Yuter et al. 2000; Kollias et al. 2004; Serpetzoglou et al. 2008; and others) focusing on the marine Scu cloud fraction. Jakob (1999) compared the cloud cover in the European Centre for Medium-Range Weather Forecasts (ECMWF) reanalysis (ERA) system with observations from the International Satellite Cloud Climatology Project (ISCCP) and found a model underestimation of stratocumulus cloud cover over the west coasts of subtropical continents by 15%. Duynkerke and Teixeira (2001) also used observations from the First ISCCP Regional Experiment (FIRE I) to determine that the cloud cover in ERA is strongly underestimated. They argued that, in a CGCM, underestimates of Scu cloud cover can lead to warmer than usual SST because of excessive solar radiation at the surface, which may also feedback to give fewer Scu clouds.

This study focuses on the southeast Pacific (SEP) Scu regime that extends from the equator southward for about 1500 km to central Chile (Klein and Hartmann 1993). This cloud deck persists year-round and has an impact on El Niño–Southern Oscillation (ENSO) and on the continent (Garreaud et al. 2001). Despite its importance to the global climate and spatial morphology, the SEP Scu regime has received little attention till the end of last century (Serpetzoglou et al. 2008). To study the complex air–sea interactions and the MABL structure in the Pacific cold tongue ITCZ complex (CTIC), a process study, the Eastern Pacific Investigation of Climate Processes in the Coupled Ocean–Atmosphere System (EPIC) was conducted in 2001 (Bretherton et al. 2004). Under this study the Woods Hole Oceanography Institute's (WHOI) Upper Ocean Process (UOP) group deployed an Ocean Reference Station (Stratus ORS) near the annual maximum of stratus cloud cover in October 2000. The Stratus ORS is located at 20°S, 85°W and has collected observations of broadband radiative fluxes and surface meteorological parameters continuously since it was launched. Following EPIC, the Stratus ORS has been maintained under the National Oceanic and Atmospheric Administration's (NOAA) Climate Observation Program (COP) and serviced each year.

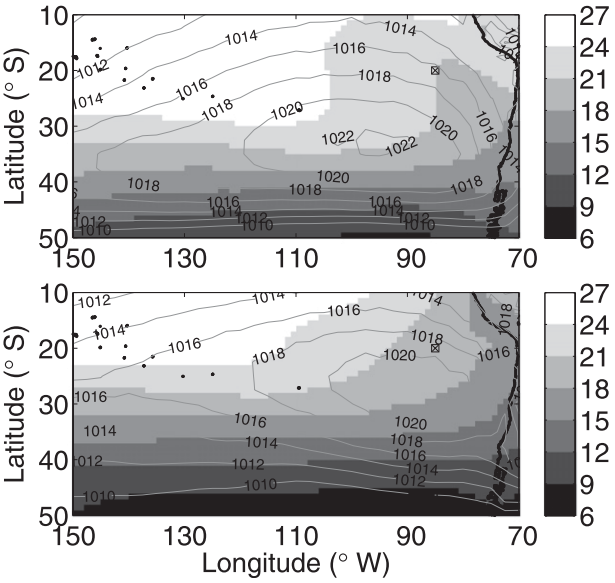

FIG. 1. Average sea surface temperature (shading, °C) and sea level pressure (contours, mb) from the NCEP reanalysis–derived data for (top) DJF and (bottom) JJA. Stratus ORS location is shown by a cross in a square.

The location of the Stratus ORS relative to the SST and pressure fields for December–February (DJF) and June–August (JJA) averaged from January 2001 to December 2005 are shown in Fig. 1. The SST fields are monthly averages from the NOAA Optimum Interpolation version 2 dataset (OI V2 SST) (Reynolds et al. 2002), and the pressure fields are monthly averages from the National Centers for Environmental Prediction (NCEP) reanalysis dataset (Kalnay et al. 1996). The plots in Fig. 1 correspond to Southern Hemisphere summer (top) and winter (bottom). In the summer, the temperatures are warmer with the subtropical high pressure system centered at around 32°S and 95°W. As expected in the winter, the temperatures decrease as the high pressure system is centered more northward. The shifting of this subtropical high pressure system and the changes in the associated wind fields is one of the major factors in maintaining a strong temperature and moisture inversion in the MABL and produces conditions conducive for the formation of Scu clouds (Xu et al. 2005).

The focus of this study is on the changes in the cloud cover on monthly to seasonal time scales that could be due to changes in the aerosol loading in the region (Stevens et al. 2003; Sharon et al. 2006; and others), changes in the lower-tropospheric stability (Klein and Hartmann 1993), or the shifting of the subtropical high

pressure system (Xu et al. 2005; and others). There are relatively few long-term in situ surface observations for this climatically important region that can provide a climatology of the surface meteorology and fluxes along with estimates of cloud fraction. Furthermore, there are few long-term estimates of the diurnal variability of the low-level clouds observed at the ORS and the surrounding over ocean environment. Thus there is a lack of direct observations for the verification and evaluation of model representations of this region.

In this study we present climatology of the SEP region using data from the Stratus ORS, collected during January 2001 to December 2005. The annual cycle of the surface meteorological parameters and surface fluxes is presented in section 2. Cloud fraction is determined using a simple model in section 3. Annual and diurnal changes in the cloud radiative forcing are discussed in section 4. The paper is concluded with a summary and a discussion of the correlations of the annual cycle of derived cloud fraction to that of other parameters.

2. Surface meteorology

The Stratus ORS has been collecting data continuously since October 2000. The complete suite of instruments and their performance is described in detail by Colbo and Weller (2009), with additional information available in Hosom et al. (1995), Payne et al. (2002), and Cronin et al. (2002). The measurements include surface downwelling shortwave and longwave radiative flux, wind speed and direction, air temperature, relative humidity, barometric pressure, rain rate, and sea surface temperature. Hourly values of these parameters are reported on a near-real-time basis. Since the aim of this study is to develop a climatology of variables suitable for climate studies, it was necessary to filter out small-scale extremes from the observed data. Thus, as a first step, all the hourly data values outside twice the standard deviation from the mean within a month were filtered out. After this, averages were computed on monthly basis for the whole 5 yr. The annual cycles of the parameters were obtained by averaging the time series of all 5 yr.

Figure 2 shows the mean annual cycle of surface air temperature, SST, relative humidity (RH), specific humidity (q), saturation specific humidity (q_s), pressure, and wind speed. The surface air temperature is lower than the SST throughout the year, partly because of advection of colder air throughout the year from the southeast (Fig. 3) and radiative cooling in the boundary layer. The air–sea temperature difference is maximum in July (1.4°C) and minimum in January (0.3°C). Both show a relative maximum in March, but the minimum of SST is in October, while that of air temperature is in

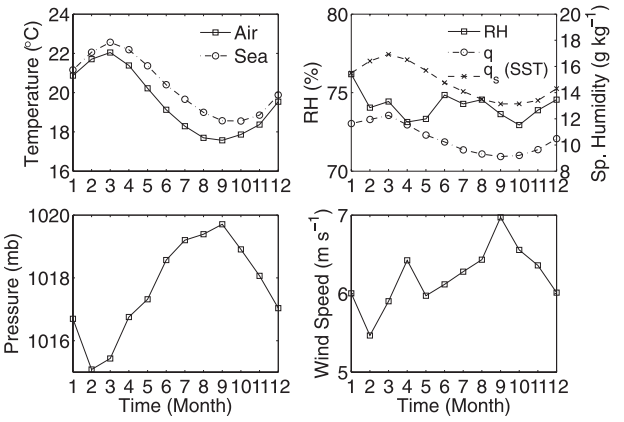

FIG. 2. Annual cycle of (top left) surface air temperature and SST; (top right) surface RH, specific humidity (q), and saturation specific humidity using SST (q_s); (bottom left) surface pressure; and (bottom right) wind speed as observed by the Stratus ORS.

September. The RH does not show a distinct sinusoidal variability as seen in the temperature and varies over a small range of 73%–77% with a semiyearly variability. The specific humidity, however, shows a sinusoidal cycle similar to the air temperature and to the surface saturation specific humidity. The changes in mixing ratio are primarily governed by the sea–air temperature difference, wind speed, and the temperature and moisture advection. The pressure variations at Stratus ORS reflect changes in the location and the intensity of the subtropical high pressure system discussed previously and shown in Fig. 1. The pressure variation is correlated negatively with the SST (−0.86) and air temperature (−0.95). The wind speed and wind direction (not shown) show little variability throughout the year. The mean wind speed is 6.2 m s^{-1} and the mean wind direction is 125°. Wind speeds vary from about 5.5 to 7 m s^{-1} with distinct peaks in April and September. Hence, the surface flow is from the southeast year-round and advects colder and drier air into the Stratus ORS area.

The surface turbulent fluxes were calculated using the Coupled Ocean–Atmosphere Response Experiment (COARE) bulk air–sea flux algorithm (Fairall et al. 1996). The sensible, virtual sensible, and latent heat flux annual cycle is shown in Fig. 3. The sensible and virtual sensible heat fluxes exhibit a Gaussian shape with peaks of about 10 and 20 W m^{-2}, respectively, during the month of July. The annual cycle of lifting condensation level (LCL) and convective velocity scale (w_*) is also shown. The LCL values were calculated using the formulation by Bolton (1980). The w_* values were calculated using the formulation given by Stull (1988), using the surface virtual sensible heat flux and the LCL as the scaling height. Thus, in this application, w_* provides a scaling parameter for the surface flux generation of

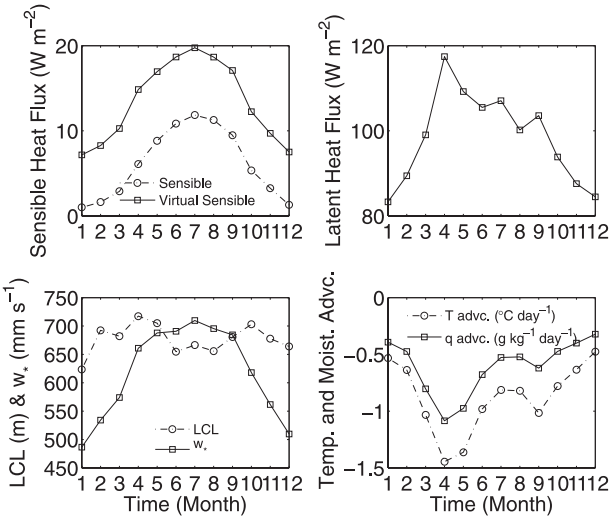

FIG. 3. Annual cycle of (top left) surface sensible and virtual sensible heat flux; (top right) latent heat flux; (bottom left) lifting condensation level and convective velocity scale; and (bottom right) temperature and moisture advection at Stratus ORS.

turbulence in the subcloud layer and does not include the effects of turbulence generated by other processes in the boundary layer. Since the LCL, which closely mirrors the surface relative humidity, varies little seasonally, w_* is mostly a reflection of the surface virtual heat flux. The values of w_* vary from 0.5 to 0.7 m s^{-1} and indicate that the surface fluxes, which are strongly driven by the advective processes, play an important role in the turbulent kinetic energy (TKE) budget of the subcloud layer in the study area. This suggests that the variations in the velocity scale are primarily due to changes in the surface heating and other factors causing it rather than the changes in the mixed layer (subcloud layer) depth. The latent heat flux peaks at about 120 W m^{-2} in April and then drops the rest of the year to a minimum of 85 W m^{-2} in January. The April maximum results since the q and q_s (SST) differences are the greatest at this time. These differences are about three months out of phase with the air–sea temperature differences.

The surface temperature advection was estimated using the NOAA OI V2 SST gridded dataset and the buoy-measured winds with the assumption that the horizontal gradient of the SST can be used as a proxy for the horizontal gradient of surface air temperature. The moisture advection was estimated by using the same temperature assumption and assuming that the relative humidity observed at the buoy was that observed in the area surrounding the buoy. Thus the moisture advection estimates closely follow the temperature advection estimates, since relative humidity has only a small range of variability. Monthly averaged values were used for the advection estimates. The maximum dry and cold advection (most negative values) is observed in April, when the buoy winds show a relative maximum. A secondary maximum occurs in September at the time of the maximum in the wind speed. The minimum cold and dry advection occurs in January, with a secondary minimum in July and August. The annual cycle of latent heat flux is negatively correlated with the temperature and moisture advection with a correlation coefficient of −0.91 and −0.85, respectively, which is consistent with the modulation of the fluxes by the local changes in humidity forced by the advection. Since the monthly latent heat flux is out of phase with the virtual sensible heat flux, these results indicate that both temperature advection and subcloud layer radiative cooling may help maintain the observed air–sea temperature differences.

3. Cloud fraction

The Stratus ORS observations have been pivotal in understanding the air–sea interaction and the associated meteorology in that region (e.g., Cronin et al. 2006). In addition, there have been yearly Stratus ORS maintenance cruises from 2000 to 2007 (except 2002) conducted in the region that included a complete set of instruments from the Physical Science Division (PSD) of NOAA/Earth System Research Laboratory (ESRL). Data from these maintenance cruises have been basis of many studies (e.g., Serpetzoglou et al. 2008; Comstock et al. 2005; and others) and have opened new avenues to study the complex aerosol–cloud–drizzle interactions in the region. But since the cruises are conducted for a month every year, long-term statistics of cloud fraction (CF) are not directly available. Hence, an attempt is made to derive the CF from the Stratus ORS observed surface parameters.

a. Calculation of cloud fraction

The surface-measured value of downwelling longwave radiative flux (LWD) is strongly influenced by the cloud-emitted longwave radiation (LW_{cld}) that is substantially higher than the clear-sky longwave radiation (LW_{clr}). Assuming one-dimensionality, these three parameters can be related to each other to first order as

$$\mathrm{LWD} = \mathrm{CF} \times \mathrm{LW}_{\mathrm{CLD}} + (1 - \mathrm{CF}) \times \mathrm{LW}_{\mathrm{clr}}. \quad (1)$$

The above equation can be used to estimate the CF from the Stratus ORS-measured LWD and modeled estimates of LW_{cld} and LW_{clr}. The cloud-emitted longwave radiation (LW_{cld}) was modeled by assuming that cloud emits as a blackbody, emitting radiation at the LCL temperature (see appendix). This assumption may result

in an overestimate of LW_{cld} in cases where there is strong decoupling of MABL.

The clear-sky downwelling longwave radiative flux (LW_{clr}) is estimated using a formulation developed by Fairall et al. (2008), which is based on observations from cruises conducted in the east Pacific region between 10°N and 10°S. The scheme represents the flux as a function of surface temperature (T_{sfc}), surface specific humidity (q_{sfc}), and column-integrated water vapor (IV) and includes a latitudinal dependence. This parameterization was modified for the Stratus ORS location (20°S, 85°W) and data used in this study (see appendix). The formulation used is

$$LW_{clr} = (0.77 + 0.006\sqrt{q_{sfc}} + 0.0063 \times IV)\sigma T_{sfc}^4, \qquad (2)$$

where q_{sfc} is in grams per kilogram, IV in centimeters, and T_{sfc} in kelvins. Monthly values of surface temperature and humidity from the Stratus ORS were used with monthly IV estimates from the Special Sensor Microwave Imager (SSM/I) dataset.

To evaluate the CF formulation from Eq. (1), it was applied to observations from two Stratus ORS maintenance cruises—the Eastern Pacific Investigation of Climate Processes in the Coupled Ocean–Atmosphere System (EPIC) in 2001 (Bretherton et al. 2004) and Pan American Climate Study (PACS) in 2003 (Kollias et al. 2004). The infrared flux and thermodynamic data used in the calculations were from the NOAA/ESRL flux suite on board the research vessels. The calculated hourly CF along with the ceilometer-derived hourly zenith cloud fraction for these two cruises are shown in Fig. 4.

The model-derived CF agrees well with the ceilometer-derived zenith cloud fraction and has a correlation coefficient of 0.86 for the EPIC cruise and of 0.92 for the PACS 2003 cruise. Similar analysis done for ORS maintenance cruises during other years that had more boundary layer (BL) decoupled conditions (2006) showed high correlations (0.92) too. The high correlation values of the observed and model-calculated CF during both coupled and decoupled BL conditions suggests that the model can be applied to a larger dataset to get multiyear cloud climatology. Although the derived cloud fraction and the ceilometer-observed zenith cloud fraction have high correlation, they differ from each other in the absolute value of cloud fraction. This is mainly because the derived cloud fraction uses the pyrgeometer-measured downwelling longwave radiative flux that has a hemispheric field of view, while the ceilometer is a vertically pointing laser instrument with a very narrow field of view.

The accuracy of this method depends on a limited modulation of the observed downward radiation by

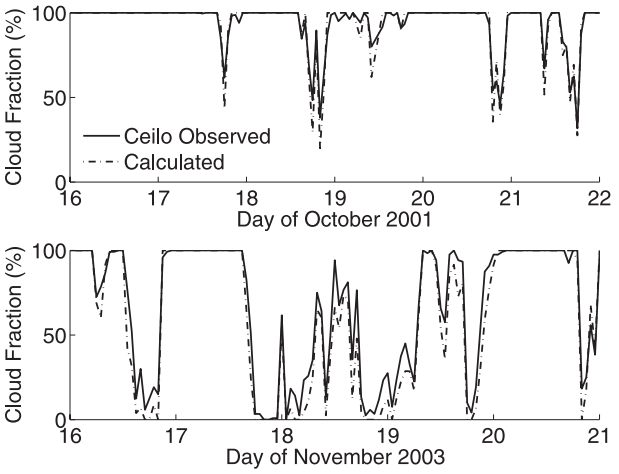

FIG. 4. Comparison of the derived cloud fraction and ceilometer-observed zenith cloud fraction for (top) EPIC 2001 and (bottom) PACS 2003. The observed and calculated cloud fractions show a correlation of 0.86 and 0.92 during EPIC 2001 and PACS 2003, respectively.

factors not represented in the formulation. Cirrus clouds, for example, could contribute to increases in the downwelling longwave radiative flux at the top of the boundary layer. Upper-level clouds would have the greatest impact when there are few low-level clouds. But previous studies have shown that the cirrus cloud cover over the SEP region is less than 5% year-round with little variation (Wylie et al. 2005). Minnis and Harrison (1984) also reported little difference between low-cloud amounts and total cloud amount in the area of interest. In addition, few high-level clouds were observed during any of the Stratus ORS maintenance cruises from the cloud radars on board. Hence we expect the error induced by high-level clouds to be minimal. For small CF (~20%), a 5 W m^{-2} bias in LW_{clr} would cause about a 10% bias in the CF.

For high CF conditions, the largest source of uncertainty will be the LW_{cld} estimate. A 5 W m^{-2} uncertainty, which is equivalent to about 2.7°C uncertainty in the effective radiative temperature of low-cloud cloud bases, will result in about a 4% uncertainty in the CF estimate. If this uncertainty is random, then averaging will minimize this effect on the estimated CF. The good correlation between the observed CF and that estimated from Eq. (2) for the two Stratus ORS cruises (shown in Fig. 4) indicates that the errors in the parameterization are minimal for these two cases.

The above technique was applied to the Stratus ORS dataset from January 2001 to December 2005. The technique was applied to monthly values of the observed parameters, since we intend to develop a monthly climatology of Scu cloud cover and other parameters. Also at hourly and daily time scales the Scu systems are

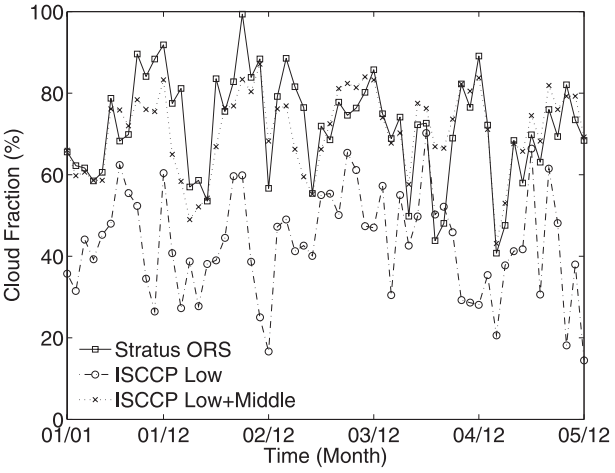

FIG. 5. Monthly averaged Stratus ORS-derived cloud fraction and ISCCP monthly averaged low- and low- plus middle-cloud cover at the Stratus ORS location.

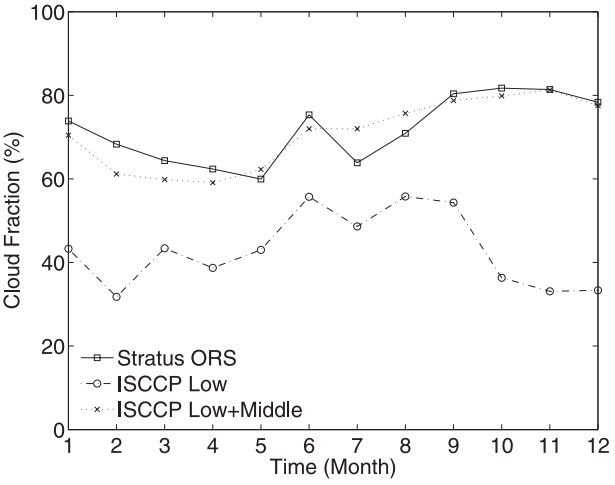

FIG. 6. Annual cycle of Stratus ORS–derived cloud fraction and ISCCP low-cloud cover and ISCCP low- plus middle-cloud cover.

strongly modulated by synoptic disturbances rather than large-scale features (Garreaud et al. 2001). Although the averaged values of all the parameters were used, the maximum value of the LCL temperature for the entire month, which corresponds to the lowest cloud base, was used for the LW_{cld} estimate (see appendix). The derived monthly averaged CF values are shown in Fig. 5. Also shown are the low-cloud cover and low- plus middle-cloud cover values from the ISCCP visible and IR combined D2 level dataset (Rossow and Schiffer 1991; Rossow et al. 1989; Rossow and Garder 1993). Although, clouds observed at the location fall in the low-cloud category of the ISCCP cloud types ($P > 680$ mb), the derived cloud cover differs substantially from the ISCCP low-cloud cover. The low plus middle ISSCP cloud cover is much closer to that estimated from the buoy.

Figure 6 shows the average annual cycle of Stratus ORS–derived CF along with that of ISCCP (visible + IR D2 level)-derived low- and low- plus middle-cloud cover from 2001 to 2005. The annual variation of the cloud cover is small with a range of about 20%. CF is highest in October with a minimum in May. There is a sharp peak in the Stratus ORS CF observed in the month of June during all years except 2004. In 2004, the CF is high during both May and June compared with the April and July CF. The ISSCP estimates also indicate a relative maximum in June. The ISCCP low plus middle CF shows a high correlation (0.86) with the Stratus ORS CF estimates, in contrast to the ISCCP low-cloud cover, which is substantially lower than those calculated and shows little correlation (-0.08) with the Stratus ORS estimates.

The annual cycle of Stratus ORS–derived CF is different than the annual cycle of CF as reported by Klein and Hartmann (1993) using surface weather observations and by Leon et al. (2008) using *CloudSat* and Cloud-Aerosol Lidar and Infrared Pathfinder Satellite Observations (CALIPSO). The annual cycle of CF reported by Klein and Hartmann (1993) peaks at about 70% in September–November (SON) and has a minimum of about 40% in DJF. It is difficult, however, to compare the ORS-derived annual cycle of CF to that reported by Klein and Hartmann (1993) because of the differences in temporal resolution, spatial resolution, and the definition of CF between the two. Although the amplitude and phase of the ORS-derived annual cycle of CF compares favorably with that reported by Leon et al. (2008), the two differ by about 20% in their mean value, with the latter being lower. The difference is mainly due to instrument sensitivity, the low number of samples used, and a larger area used in CF calculation in the later study.

The difference between the Stratus ORS–derived CF and the ISCCP-derived low-cloud cover is not constant but varies year-round. The difference is a maximum in December and a minimum in June. These results indicate that the ISCCP algorithm may be misclassifying some of the low clouds into the middle-cloud category. The objective of this comparison is not to provide an alternative technique for calibrating ISCCP-derived low-cloud CF. The plot is shown for comparison with other independent observations. Furthermore, previous modeling studies (e.g., Jakob 1999; Bachiochi and Krishnamurti 2000; Gordon et al. 2000; Mochizuki et al. 2007; and others) have compared their model results with the ISCCP-derived low-cloud CF. The ISCCP algorithm misclassifying some of the low clouds into midlevel cloud category has been reported previously by Minnis et al. (1992) and by Garay et al. (2008). Furthermore,

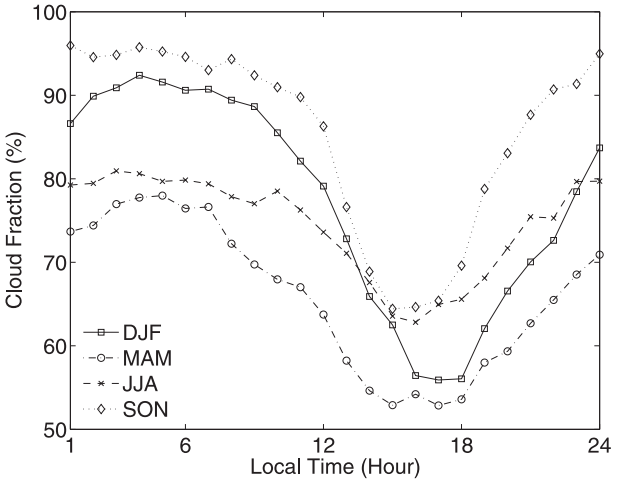

FIG. 7. Diurnal cycle of cloud fraction at the Stratus ORS for different seasons averaged for the 2001–05 period.

all the data collected by *CloudSat* and CALIPSO till October 2008 in the vicinity of ORS (~100 km) were analyzed and no clouds or cloud-top heights were observed that can be classified as midlevel clouds according to ISCCP classification. This, along with the high correlation of ISCCP low- plus midlevel cloud cover with the calculated CF, suggests that the ISCCP algorithm is able to observe the low clouds over the buoy location but is misclassifying some of them in the midlevel category. This may be due to the dependence of ISCCP algorithm on low-resolution observations of the atmospheric temperature structure in that region (Garay et al. 2008; Wang et al. 1999). It is beyond the scope of this study to further analyze the reason for this misclassification in the ISCCP algorithm or to provide a correction for it.

There are pronounced diurnal changes in the Scu CF because of its modulation by the solar radiation (Minnis and Harrison 1984; Rozendaal et al. 1995) and by the changes in the surface divergence field and large-scale vertical velocity (Garreaud and Munoz 2004; Xu et al. 2005). The diurnal cycle of Scu CF was obtained for each month in 2001–05 from the diurnal cycle of the observed parameters used in the technique. Monthly averaged values for each hour were used to make these estimates. These monthly diurnal cycles were then averaged for the 5 yr to obtain mean monthly diurnal cycle. Figure 7 shows the seasonally averaged diurnal cycle of Scu CF. The maximum cloud cover is observed during SON, while minimum occurs during March–May (MAM). The SON diurnal cycle compares well with that from the Geostationary Operational Environmental Satellite (GOES) retrievals of Minnis and Harrison (1984) with an amplitude of about 30% and similar maxima and minima time. The Stratus ORS–observed CF diurnal cycle for this period, however, shows a more skewed cycle with a sharp minimum and a broader maximum.

TABLE 1. Range, phase, and mean nighttime value of the seasonally averaged diurnal cycle of cloud fraction.

Months	Range	Phase	Mean nighttime
DJF	0.36	17	0.89
MAM	0.25	17	0.75
JJA	0.18	16	0.80
SON	0.31	15	0.95

The CF peak-to-peak variation is a maximum (39%) during the summer months of DJF, and is minimum (18%) during the winter months of JJA. The character of the maxima and minima also show seasonal variations. There is a distinct minimum during all seasons, but not a distinct maximum. The time of the minimum also changes seasonally suggesting further the role that the diurnal variation in the divergence field (e.g., Minnis and Harrison 1984; Garreaud and Munoz 2004) may have in modulating the character of the diurnal changes in CF. Although shown are the seasonally averaged diurnal cycles, changes in magnitude of order of 10% from hour to hour are visible in the diurnal cycle of SON and DJF. Changes greater than 15% in an hour are observed during October.

The diurnal cycle of CF is summarized in Table 1. The range, phase, and mean nighttime value of the diurnal cycle are tabulated for each season. The range is defined as the difference between the maximum and minimum value. The phase of a cycle is defined as the time of occurrence of the minimum value, since the maximum tends to relatively broad and flat. The mean nighttime value is the average from 2300 to 0700 local time (defined as 6 h behind UTC).

Figure 8 shows the annual cycle of Scu CF and the annual cycle of nighttime-only Scu CF. The difference between these two indicates the modulation of the daily CF by incoming solar radiation, surface divergence field, and large-scale vertical velocity. The difference is maximum in October (12%), while the minimum occurs in June at the time of the winter solstice. The sharp peak in the CF during June is also seen in the nighttime CF, although June also has the minimum amplitude in the diurnal cycle. The range of the diurnal cycle for each month is highly correlated with the difference between the nighttime and total cloud fraction (0.89). The amplitude of the diurnal variation is greatest in February and decreases to a minimum in June. There is a large increase in the diurnal variability of the October CF compared with that in September. This increase also

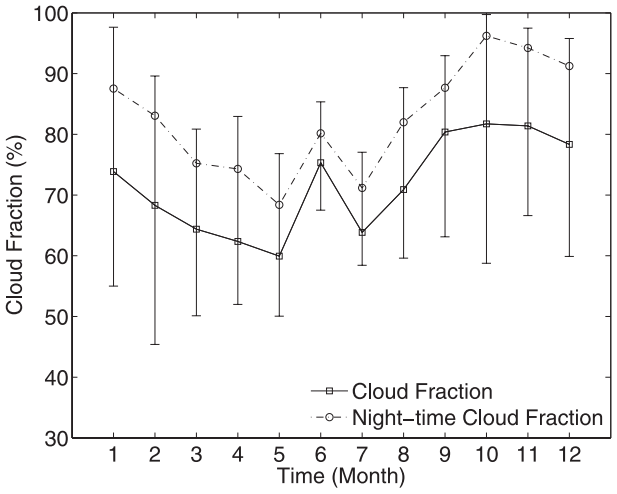

FIG. 8. Annual cycle of averaged cloud fraction along with averaged nighttime-only cloud fraction. Cloud fraction was averaged between 2300 and 0700 local time to derive the nighttime cloud fraction. The vertical bar indicates the average range of monthly diurnal cycle.

affects the difference between nighttime and total CF. The reason for this increase is not clear and requires further analysis. These observations indicate that the neglect or misrepresentation of the diurnal effects in a model can introduce an error of up to 15% in the monthly CF during the summer months.

b. Correlation analysis

Ranging from full physics shallow cumulus parameterizations (e.g., Bretherton et al. 2004; and others) to simple criteria defining lower-tropospheric stability (Klein and Hartmann 1993; and others), many criteria are used to parameterize Scu CF in GCMs. Here we present correlation coefficients of the average annual cycle of Scu CF with the average annual cycle of other parameters. They are tabulated in Table 2. Also tabulated are the correlation coefficients between the annual cycle of mean nighttime CF and the annual cycle of the parameters, since the mean nighttime CF represents conditions unperturbed by solar heating. Since the correlation coefficients are calculated using the averaged annual cycle of the parameters, the low number of samples (12) used yields low confidence in the calculated correlation coefficients. The authors will like to emphasize that the calculations are not presented to be used in a model parameterization of Scu CF or to test any model parameterization as done by (Klein 1997; Klein et al. 1995) but to determine the factors that have a close coupling to the Scu CF. Since the confidence level in all the determined correlation coefficients is same, they can be used to judge the relative importance of a parameter to CF as compared with the others.

The SST (and surface air temperature) is negatively correlated to the cloud fraction and positively correlated to the net radiative CRF. Thus the largest cooling effects at the surface due to clouds occur when the SSTs are the lowest. The surface air temperature and specific humidity are also negatively correlated to CF as they are heavily influenced by the SST and sea–air temperature difference, respectively.

The lifting condensation level (or equivalently the relative humidity) and the convective velocity scale (or equivalently the virtual heat flux) do not show a significant correlation with the cloud fraction. Stronger heat fluxes at the surface would enhance turbulent mixing in the lower part of the layers, but this appears to have no affect on the cloudiness. Some of the clouds observed in this area are undoubtedly associated with decoupled

TABLE 2. Correlation coefficients of the annual cycle of various parameters with the averaged annual cycle of cloud fraction and averaged annual cycle of nighttime-only cloud fraction.

Parameter	Correlation coefficient with cloud fraction	Correlation coefficient with nighttime cloud fraction
Sea surface temperature	−0.73	−0.69
Air temperature	−0.58	−0.52
Specific humidity	−0.55	−0.49
Lifting condensation level	−0.30	−0.21
Large-scale subsidence	0.09	0.04
700-mb potential temperature	−0.09	−0.01
Surface potential temperature	−0.57	−0.51
Surface moisture advection	0.69	0.69
Surface temperature advection	0.60	0.61
Sensible heat flux	−0.20	−0.32
Latent heat flux	−0.59	−0.63
Convective velocity scale	−0.30	−0.38
Klein stability parameter	0.87	0.83
Estimated inversion strength	0.70	0.72

boundary layers (Serpetzoglou et al. 2008). Thus, although the LCL shows little variability during the year, it may not reflect cloud-base height variability.

The large-scale vertical velocity at 700 mb from NCEP reanalysis data shows negligible correlation with cloud fraction. This result is consistent with a study by Slingo (1980) where subsidence was found to be a poor indicator of Scu cloud amount. The lack of correlation of CF with large-scale vertical velocity maybe real but could also be misleading since the large-scale vertical velocity in the NCEP reanalysis dataset is loosely constrained by observations over the southeast Pacific region. Surface temperature and moisture advection show a positive correlation (>0.60) with cloud fraction. The advection at the location is from the southeast year-round and brings colder and drier air to the buoy. Hence, the net effect of advection is to reduce the near-surface air temperature and specific humidity and enhance the surface fluxes.

The surface latent heat flux is negatively correlated with the cloud fraction. The flux increase with the CF is due to increases in the air–sea differences in mixing ratio. The negative correlation of the surface moisture flux with the fractional cloudiness is also consistent with the negative correlation between mixing ratio and CF. The latent heat flux is also negatively correlated to the surface temperature and moisture advection.

A relationship between the low-level cloud amount and a measure of lower-tropospheric stability has been used in some simple GCM boundary layer cloud parameterizations (Randall et al. 2007). One such measure of the lower-tropospheric stability proposed by Klein and Hartmann (1993) (the Klein stability parameter) has been widely used (Miller 1997; Rasch and Kristjansson 1998; and others). The Klein stability parameter is defined as difference between the 700-mb potential temperature (θ_{700}) and surface potential temperature (θ_{sfc}). Some modifications for improving this parameterization have also been proposed (e.g., Wood and Bretherton 2006; Mochizuki et al. 2007; and others).

For calculating the Klein stability parameter, the Stratus ORS–observed surface potential temperature was used along with the 700-mb potential temperature from the NCEP reanalysis dataset. It can be seen that the annual variability in the CF is highly correlated with the Klein stability parameter. The estimated inversion strength (Wood and Bretherton 2006), which is a modification of the Klein stability parameter, is less correlated with CF than the Klein stability parameter. Most of the correlation of CF with the stability parameter is due to the surface potential temperature rather than the 700-mb potential temperature. However, the correlation with the Klein factor is still higher than that with the surface potential temperature alone. The surface potential temperature is strongly modulated by the temperature of the sea surface.

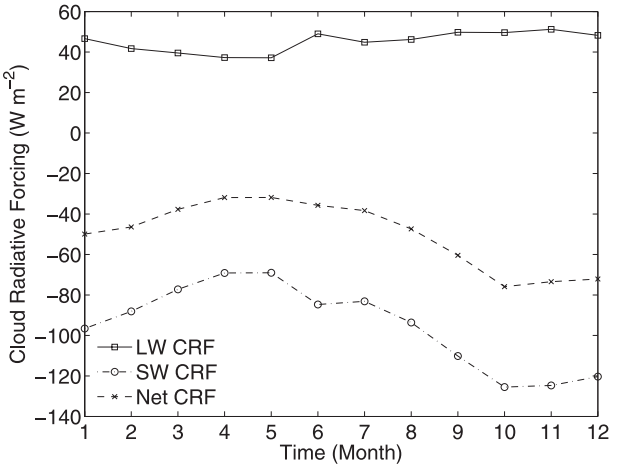

FIG. 9. Annual cycle of surface longwave, shortwave, and net cloud radiative forcing at the Stratus ORS.

4. Surface cloud radiative forcing

To quantify the impact of these clouds on the surface energy budget, we calculated surface longwave (LW) and shortwave (SW) cloud radiative forcing (CRF). CRF is calculated by subtracting the modeled clear-sky value from the observed flux values at the surface (Cronin et al. 2006; Fairall et al. 2008). The clear-sky downwelling shortwave radiative flux was calculated using the method described by Cronin et al. (2006) that uses the solar constant from Lean (1997) and the transmission properties of atmosphere as parameterized by Iqbal (1988). More details can be found in Cronin et al. (2006) and Hare et al. (2005). The annual cycle of LW, SW, and net CRF are shown in Fig. 9. It is evident that these clouds are efficient reflectors of the incoming shortwave radiation since during the summer months of DJF the SW CRF is about -120 W m^{-2}. But the clouds have a small positive effect on the surface longwave budget as annual mean LW CRF is around 45 W m^{-2}. The net CRF and hence the impact of these clouds on the surface radiation budget is around -50 W m^{-2}, indicating that these clouds have a net cooling effect on the sea surface below. The results presented in this section are consistent with those of Cronin et al. (2006) and provide further validation of the clear-sky longwave radiation parameterization.

Figure 10 shows the diurnal cycle of the LW and SW CRF. The LW CRF has minimum at about 1600 local time during all seasons. Although there is a distinct

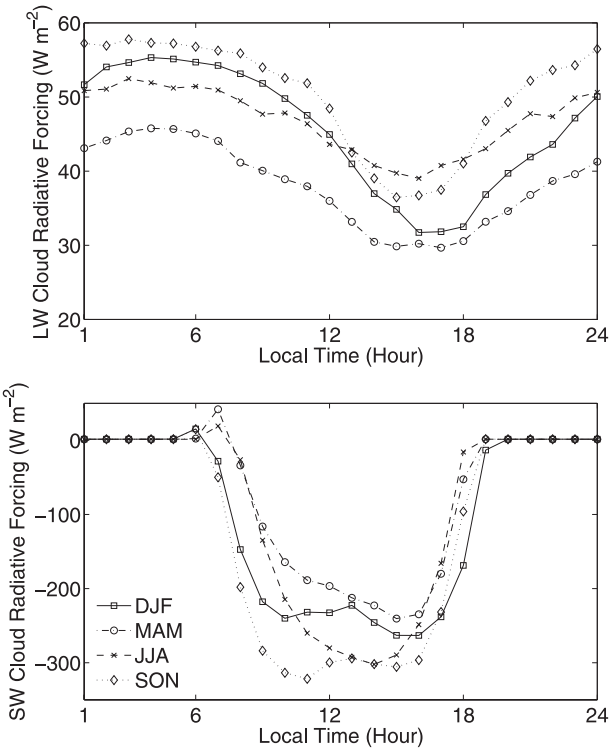

FIG. 10. Seasonally averaged diurnal cycle of (top) longwave and (bottom) shortwave cloud radiative forcing at the Stratus ORS.

minimum during all seasons, there is no distinct maximum implying that the cloud cover and SST remain fairly constant at night. The mean nighttime LW CRF has minimum during MAM that is consistent with a higher LCL height during those months than other. The range of the LW CRF is smallest during JJA but highest during DJF.

The SW CRF exhibits the shape of an inverted Gaussian curve during all seasons. The sunrise is at about 0700 local time. There a small positive SW cloud forcing seen during the sunrise period suggesting scattering by aerosols and a solid deck of Scu clouds. During DJF and SON an increase in SW cloud forcing is seen at 1300 local time. This increase suggests that more downwelling SW radiation is received at the surface. This is due to a sharp decrease in cloud cover during that hour compared with others (Fig. 7). DJF and SON are seasons with higher cloud cover (74% and 82%, respectively) compared to MAM and JJA (62% and 70%, respectively), and hence this peak in the SW CRF is more pronounced during these seasons. Note that the absolute (not normalized) values of SW CRF are shown, and hence from these values it is difficult to assess if the seasonal changes are due to changes in cloud properties among different seasons or changes in the incoming solar radiation. The diurnal cycle of SW and LW CRF is tabulated in Table 3. The range, phase, and mean nighttime value of the cycle are documented. The results presented in this section are consistent with previous studies (e.g., Cronin et al. 2006). Since CRF in this study includes longer time observations than those in previous studies, the purpose of this analysis is to describe the details of the annual and diurnal cycle of the CRF but not to compare these observations with model outputs.

5. Summary and conclusions

Climatology of surface meteorology, surface fluxes, cloud fraction, and cloud radiative forcing of the SEP region is presented based on data from the Stratus ORS from 2001 to 2005. The RH remains constant throughout the year, although the SST and surface air temperature exhibit a sinusoidal annual variability that is negatively correlated with the surface pressure. The surface sensible heat flux varies little year-round, while the surface latent heat flux has an annual range of 40 W m^{-2} and is highly correlated with the advection of cold and dry air.

A simple model was used to derive monthly cloud fraction from the surface temperature, specific humidity, column-integrated water vapor, and downwelling longwave radiative flux. The sum of the ISCCP visible and IR combined low and middle CF retrievals at the buoy shows excellent correlation with the Stratus ORS–derived CF, while the ISCCP low-cloud CF showed negligible correlation. The annual cycle of CF shows persistent cloud cover year-round with a minimum in May and a maximum in October. A sharp peak in the CF is observed in the month of June for all the 5 yr except 2004, when the CF is high during May and June compared with April and July. The peak might be due to

TABLE 3. Range, phase, and mean nighttime value of seasonally averaged diurnal cycle of shortwave and longwave cloud radiative forcing.

	Range (W m^{-2})		Phase (local hour)		Mean nighttime (W m^{-2})	
Months	SW CRF	LW CRF	SW CRF	LW CRF	SW CRF	LW CRF
DJF	279	24	16	16	—	54
MAM	282	16	15	17	—	44
JJA	321	13	14	16	—	51
SON	337	21	11	15	—	57

shifting of the subtropical high relative to the buoy location or changes in the aerosol loading in the region from the continental boundary. A similar peak of a weaker magnitude is also seen in mean annual cycle of the ISCCP total cloud fraction.

As argued by previous studies, there is a modulation of these clouds by solar radiation, and hence they exhibit a diurnal cycle. The diurnal cycle shows minima in late afternoon, although there is no distinct maximum seen in the cycle. The highest values in the diurnal cycle are observed during night and correspond to the solar unperturbed cloud cover. The nighttime cloud cover is highest in SON period and lowest in JJA. The difference between averaged nighttime CF and averaged CF is minimum during the winter months of JJA and maximum during summer months of SON. The range of diurnal variations shows the same trend. The diurnal changes in CF and CRF can be very subtle with over 15% change in CF but a change of over 100 W m^{-2} in the SW CRF on hourly time scales. These diurnal changes are important for climate models to capture in order for them to simulate atmospheric physical processes such as clouds and convection (Slingo et al. 2004). The diurnal cycle of CF for this region was reported by previous studies (Minnis and Harrison 1984; Rozendaal et al. 1995) with a temporal resolution of 3 h. Hence, the intricate details of the diurnal cycle of CF (>10% changes on hourly time scales) and diurnal cycle of CRF (double minimum in SW CRF) are reported for the first time.

Surface LW CRF is positive throughout the year (~45 W m^{-2}), while the surface SW CRF is negative with minima in October (~−130 W m^{-2}) and maxima in April (~−70 W m^{-2}). The net CRF is negative throughout the year and results in a radiative cooling of the sea surface. The diurnal cycle of LW CRF varies sinusoidally with pronounced minima but less distinct maxima. The range of the diurnal cycle of LW CRF is between 30 and 60 W m^{-2} annually. The diurnal cycle of SW CRF has an inverted Gaussian shape and is always negative. The SW CRF diurnal cycle minimum is about −350 W m^{-2} for SON while about −250 W m^{-2} in MAM. There is a double minimum seen in the SW CRF diurnal cycle during DJF and SON. As the LW CRF is always positive and the SW CRF is highly negative during the day, the net CRF is negative during the day and positive at night. Hence, Scu clouds cool the sea surface below during the day by reflecting most of the incoming solar radiation and warm the sea surface at night.

Simple correlation analysis between the averaged annual cycle of CF and other parameters yielded that the Klein stability parameter, which reflects the MABL stability, and the surface latent heat flux, which is modulated by the moisture advection, are the two major factors that are correlated with the annual cycle of the Scu CF at the Stratus ORS. Figure 11 shows the annual cycle of cloud fraction, Klein stability parameter, and latent heat flux. Although the latent heat flux shows a strong negative correlation with cloud fraction, it does not capture the same level of the detail in the cloud fraction cycle as given by the Klein stability parameter. Similar to the peak in June observed in the annual cycle of CF a small jump in the Klein stability parameter is also seen during that month. Although the significance of this peak may be questionable, it owes its existence to the 700-mb potential temperature in the formulation applied here.

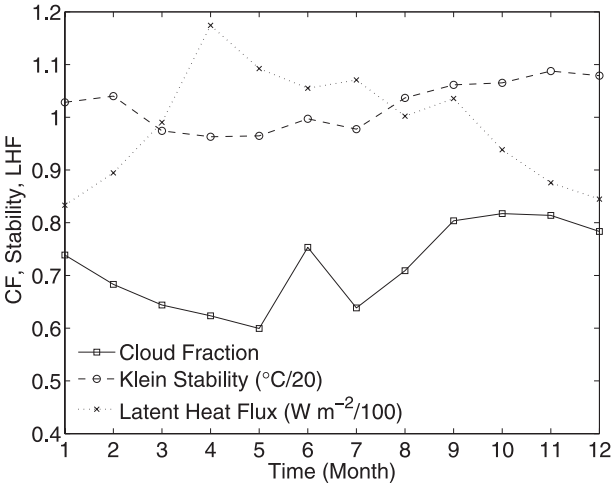

FIG. 11. Annual cycle of Stratus ORS cloud fraction, Klein stability parameter, and latent heat flux.

Although the SEP Scu regime plays an important role in the earth's radiation budget, and possibly ENSO and controlling the South American regional climate, it is poorly represented in GCMs and CGCMs. Understanding the complex air–sea and aerosol–cloud–drizzle interaction was the focus of past field experiments in the region (EPIC 2001, PACS 2003, etc.) and a principal focus of the Variability of the American Monsoon Systems (VAMOS) Program's Ocean–Cloud–Atmosphere–Land–Study (VOCALS) Regional Experiment. Although the Klein stability parameter can be used to predict the CF within certain limits on monthly to seasonal scales, it may not be a useful parameter for predicting Scu CF on daily or hourly time scales where diurnal effects dominate. Future field campaigns lasting for months and having full set of instruments on board research vessels might provide additional insights on the complexity of aerosol–cloud–drizzle interactions and be helpful in developing an Scu CF parameterization that could be used on shorter time scales.

Acknowledgments. The authors would like to thank Dr. Stephen Klein for useful discussions that helped to improve the manuscript. The reanalysis data were provided by the NOAA/OAR/ESRL PSD, Boulder, Colorado, from their Web site at http://www.cdc.noaa.gov. This research was supported by the Climate Prediction Program for the Americas (CPPA) of NOAA's Climate Program Office. The Stratus Ocean Reference Station at 20°S, 85°W is supported by NOAA's Climate Observation Program.

APPENDIX

Clear- and Cloudy-Sky Downwelling Longwave Radiative Flux Parameterization

The clear- and cloudy-sky downwelling longwave fluxes needed for Eq. (1) were estimated using parameterized simple analytical schemes.

a. Clear-sky downwelling longwave radiative flux

The clear-sky flux downwelling longwave radiative flux is parameterized using the formulation given by Fairall et al. (2008). They parameterized the flux as a function of surface air temperature, specific humidity, and column-integrated water vapor:

$$\mathrm{LW}_{\mathrm{clr}} = (A + B\sqrt{q_{\mathrm{sfc}}} - 0.0188 + 0.0063 \times \mathrm{IV})\sigma T_{\mathrm{sfc}}^4, \tag{A1}$$

$$\text{where} \quad A = 0.50 + \left(\frac{0.13}{60}\right)\mathrm{abs(latitude)} \quad \text{and}$$

$$B = 0.091 - \left(\frac{0.03}{60}\right)\mathrm{abs(latitude)}.$$

As the Stratus ORS is located at 20°S, the formulation simplifies to

$$\mathrm{LW}_{\mathrm{clr}} = (0.5212 + 0.081\sqrt{q_{\mathrm{sfc}}} + 0.0063 \times \mathrm{IV})\sigma T_{\mathrm{sfc}}^4. \tag{A2}$$

But the majority of data used in developing the Fairall et al. (2008) parameterization came from observations of these parameters between 10°S and 10°N. Since the domain of consideration in this study falls outside of where the parameterization was developed, the scheme was revaluated and the coefficients tuned based on the observations. Previous climatology studies focused on the region (e.g., Klein and Hartmann 1993; Rozandaal et al. 1995; Cronin et al. 2006) have shown that the cloud fraction has a maximum in the months of September–November of over 80% and a minimum in the months of June–August of about 60%. Hence, it can be assumed that at least 5% of the observations during all months are in cloud-free conditions. Data from the previous cruises showed that the cloudy-sky downwelling longwave radiative flux is much higher (~50 W m^{-2}) than the clear-sky downwelling longwave radiative flux. Hence the lowest 5% values of surface downwelling longwave radiative flux for each month collected by ORS can be assumed to correspond to clear-sky periods. Figure A1, shows the model-predicted clear-sky flux along with the mean of lowest 5% values of surface-measured downwelling longwave radiative flux. It can be seen that the model underestimates the flux by about 15 W m^{-2} in the summer months, giving a root-mean-square (RMS) error of 7.11 W m^{-2}.

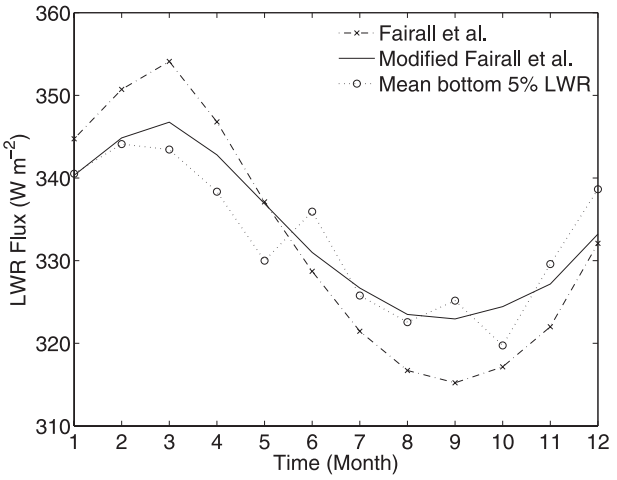

FIG. A1. Annual cycle of averaged lowest 5% of downwelling longwave radiative flux, clear-sky downwelling longwave radiative flux per Fairall et al. (2008), and clear-sky downwelling longwave radiative flux from the modified Fairall et al. formulation used in this study.

An error of 15 W m^{-2} in the value of clear-sky flux can induce an error of up to 20% in cloud fraction estimates. To provide a better fit to the observations, the coefficients A and B in the model were modified to better fit the mean of lowest 5% of observations. The formulation we derived and used in this study is

$$\mathrm{LW}_{\mathrm{clr}} = (0.77 + 0.006\sqrt{q_{\mathrm{sfc}}} + 0.0063 \times \mathrm{IV})\sigma T_{\mathrm{sfc}}^4. \tag{A3}$$

The new formulation is also shown in Fig. A1 for comparison and has an RMS error of 3.73 W m^{-2} compared with the bottom 5% of the measured downwelling longwave radiative flux.

b. Cloudy-sky downwelling longwave radiative flux

As stated earlier, the previous climatologies suggest minima in cloud fraction of about 60% and maxima of

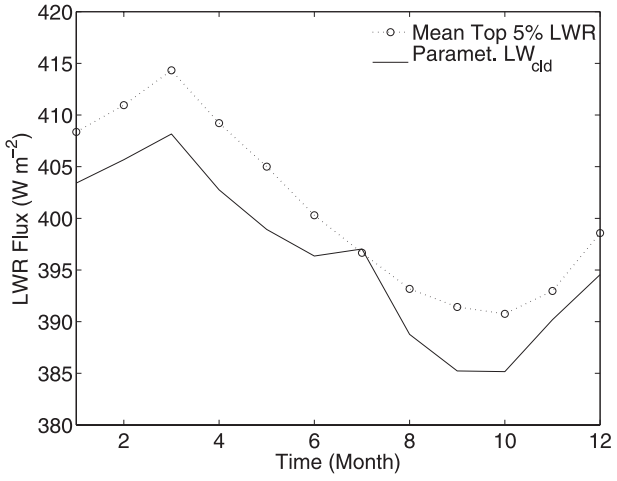

FIG. A2. Annual cycle of averaged top 5% of downwelling longwave radiative flux and the parameterized cloudy-sky downwelling longwave radiative flux.

about 80%. Hence, at least 5% of observations are collected in completely cloudy conditions. As the cloudy-sky flux is much higher than the clear-sky flux, (~50 W m^{-2}) the top 5% of the observations of downwelling longwave radiative flux collected by ORS for each month can be assumed to be taken in completely cloudy conditions. To model the cloudy-sky downwelling longwave radiative flux (LW_{cld}), we consider cloud as a perfect blackbody and assume that it is emitting radiation at the temperature of lowest LCL within a month. This is done to ensure that the flux corresponds to the thickest cloud. The comparison of the parameterization with the mean top 5% of the surface downwelling longwave radiative flux is shown in Fig. A2. It can be seen that they compare favorably with a RMS error of about 5 W m^{-2}. The LW_{cld} calculated using the mean LCL temperature had RMS error of 21.20 W m^{-2}. The observed fluxes are about 5 W m^{-2} greater than the fluxes obtained from the maximum LCL temperature blackbody values. This offset may result because, in reality, there can be additional gaseous emission from the atmospheric layer between the surface and cloud base. A 5 W m^{-2} uncertainty in the downward cloudy flux would result in about a 4% uncertainty in the CF. The same methodology used here—that is, to use the lowest/topmost 5% observations of downwelling longwave radiation as a proxy for clear-/cloudy-sky values—has been previously used by Fairall et al. (1990).

REFERENCES

Albrecht, B. A., D. A. Randall, and S. Nicholls, 1988: Observations of marine stratocumulus during FIRE. *Bull. Amer. Meteor. Soc.,* **69,** 618–626.

Bachiochi, D. R., and T. N. Krishnamurti, 2000: Enhanced low-level stratus in the FSU coupled ocean–atmosphere model. *Mon. Wea. Rev.,* **128,** 3083–3103.

Bolton, D., 1980: The computation of equivalent potential temperature. *Mon. Wea. Rev.,* **108,** 1046–1053.

Bretherton, C. S., and Coauthors, 2004: The EPIC 2001 stratocumulus study. *Bull. Amer. Meteor. Soc.,* **85,** 967–977.

Colbo, K., and R. A. Weller, 2009: Accuracy of the IMET sensor package in the subtropics. *J. Atmos. Oceanic Technol.,* **26,** 1867–1890.

Comstock, K. K., C. S. Bretherton, and S. E. Yuter, 2005: Mesoscale variability and drizzle in southeast Pacific stratocumulus. *J. Atmos. Sci.,* **62,** 3792–3807.

Cronin, M. F., N. Bond, C. Fairall, J. Hare, M. J. McPhaden, and R. A. Weller, 2002: Enhanced oceanic and atmospheric monitoring underway in eastern Pacific. *Eos, Trans. Amer. Geophys. Union,* **83,** 205, doi:10.1029/2002EO000137.

——, ——, ——, and R. A. Weller, 2006: Surface cloud forcing in the east Pacific stratus deck/cold tongue/ITCZ complex. *J. Climate,* **19,** 392–409.

Duynkerke, P. G., and J. Teixeira, 2001: Comparison of ECMWF reanalysis with FIRE I observations: Diurnal variations of marine stratocumulus. *J. Climate,* **14,** 1466–1478.

Fairall, C. W., J. Hare, and J. Snider, 1990: An eight-month sample of marine stratocumulus cloud fraction, albedo, and integrated liquid water. *J. Climate,* **3,** 847–864.

——, E. F. Bradley, D. P. Rogers, J. B. Edson, and G. S. Young, 1996: Bulk parameterization of air-sea fluxes for Tropical Ocean-Global Atmosphere Coupled Ocean–Atmosphere Response Experiment. *J. Geophys. Res.,* **101,** 3747–3764.

——, T. Uttal, D. Hazen, J. Hare, M. F. Cronin, N. Bond, and D. E. Veron, 2008: Observations of cloud radiation and surface forcing in equatorial eastern Pacific. *J. Climate,* **21,** 655–673.

Garay, M. J., S. P. de Szoeke, and C. M. Moroney, 2008: Comparison of marine stratocumulus cloud top heights in the southeastern Pacific retrieved from satellites with coincident ship-based observations. *J. Geophys. Res.,* **113,** D18204, doi:10.1029/2008JD009975.

Garreaud, R. D., and R. Munoz, 2004: The diurnal cycle of circulation and cloudiness over the subtropical southeast Pacific: A modeling study. *J. Climate,* **17,** 1699–1710.

——, J. Rutlant, J. Quintana, J. Carrasco, and P. Minnis, 2001: CIMAR-5: A snapshot of lower troposphere over the subtropical southeast Pacific. *Bull. Amer. Meteor. Soc.,* **82,** 2193–2207.

Gordon, C. T., A. Rosati, and R. Gudgel, 2000: Tropical sensitivity of a coupled model to specified ISCCP low clouds. *J. Climate,* **13,** 2239–2260.

Hare, J. E., C. W. Fairall, T. Uttal, D. Hazen, M. F. Cronin, N. A. Bond, and D. E. Veron, 2005: Cloud radiation and surface forcing in the equatorial eastern Pacific. NOAA Tech. Memo. OAR PSD 307, NOAA/ESRL, Boulder, CO, 64 pp.

Hosom, D. S., R. A. Weller, R. E. Payne, and K. E. Prada, 1995: The IMET (improved meteorology) ship and buoy systems. *J. Atmos. Oceanic Technol.,* **12,** 527–540.

Iqbal, M., 1988: Spectral and total sun radiance under cloudless skies. *Physical Climatology for Solar and Wind Energy,* R. Guzzi and C. G. Justus, Eds., World Scientific, 196–242.

Jakob, C., 1999: Cloud cover in the ECMWF reanalysis. *J. Climate,* **12,** 947–959.

Kalnay, E., and Coauthors, 1996: The NCEP/NCAR 40-Year Reanalysis Project. *Bull. Amer. Meteor. Soc.,* **77,** 437–471.

Kiehl, J. T., and P. R. Gent, 2004: The Community Climate System Model, version 2. *J. Climate,* **17,** 3666–3682.

Klein, S. A., 1997: Synoptic variability of low-cloud properties and meteorological parameters in the subtropical trade wind boundary layer. *J. Climate,* **10,** 2018–2039.

——, and D. L. Hartmann, 1993: The seasonal cycle of low stratiform clouds. *J. Climate,* **6,** 1587–1606.

——, ——, and J. R. Norris, 1995: On the relationships among low-cloud structure, sea surface temperature, and atmospheric circulation in the summertime northeast Pacific. *J. Climate,* **8,** 1140–1155.

Kollias, P., C. W. Fairall, P. Zuidema, J. Tomlinson, and G. A. Wick, 2004: Observations of marine stratocumulus in SE Pacific during the PACS 2003 cruise. *Geophys. Res. Lett.,* **31,** L22110, doi:10.1029/2004GL020751.

Lean, J., 1997: The sun's variable radiation and its relevance for earth. *Annu. Rev. Astron. Astrophys.,* **35,** 33–67.

Leon, D. C., Z. Wang, and D. Liu, 2008: Climatology of drizzle in marine boundary layer clouds based on 1 year of data from CloudSat and Cloud-Aerosol Lidar and Infrared Pathfinder Satellite Observations (CALIPSO). *J. Geophys. Res.,* **113,** D00A14, doi:10.1029/2008JD009835.

Miller, R. L., 1997: Tropical thermostats and low cloud cover. *J. Climate,* **10,** 409–440.

Minnis, P., and E. F. Harrison, 1984: Diurnal variability of regional cloud and clear-sky radiative parameters derived from GOES data. Part II: November 1978 cloud distribution. *J. Appl. Meteor.,* **23,** 1012–1031.

——, P. W. Heck, D. F. Young, C. W. Fairall, and J. B. Snider, 1992: Stratocumulus cloud properties derived from simultaneous satellite and island-based instrumentation during FIRE. *J. Appl. Meteor.,* **31,** 317–339.

Mochizuki, T., T. Miyama, and T. Awaji, 2007: A simple diagnostic calculation of marine stratocumulus cloud cover for use in general circulation models. *J. Geophys. Res.,* **112,** D06113, doi:10.1029/2006JD007223.

Norris, J. R., 1998a: Low cloud type over the ocean from surface observations. Part I: Relationship to surface meteorology and the vertical distribution of temperature and moisture. *J. Climate,* **11,** 369–382.

——, 1998b: Low cloud type over the ocean from surface observations. Part II: Geographical and seasonal variations. *J. Climate,* **11,** 383–403.

Payne, R. E., and Coauthors, 2002: A comparison of buoy meteorological systems. WHOI Tech. Rep. WHOI-2002-10, Woods Hole Oceanographic Institution, 67 pp.

Randall, D. A., J. A. Coakley, D. H. Lenschow, C. W. Fairall, and R. A. Kropfli, 1984: Outlook for research on subtropical marine stratiform clouds. *Bull. Amer. Meteor. Soc.,* **65,** 1290–1301.

——, and Coauthors, 2007: Climate models and their evaluation. *Climate Change 2007: The Physical Science Basis,* S. Solomon et al., Eds., Cambridge University Press, 589–662.

Rasch, P. J., and J. E. Kristjansson, 1998: A comparison of the CCM3 model climate using diagnosed and predicted condensate parameterizations. *J. Climate,* **11,** 1587–1614.

Reynolds, R. W., N. A. Rayner, T. M. Smith, D. C. Stokes, and W. Wang, 2002: An improved in situ and satellite SST analysis for climate. *J. Climate,* **15,** 1609–1625.

Rossow, W. B., and R. A. Schiffer, 1991: ISCCP cloud data products. *Bull. Amer. Meteor. Soc.,* **72,** 2–20.

——, and L. C. Garder, 1993: Validation of ISCCP cloud detections. *J. Climate,* **6,** 2370–2393.

——, ——, and A. A. Lacis, 1989: Global seasonal cloud variations from satellite radiance measurements. Part I: Sensitivity of analysis. *J. Climate,* **2,** 419–458.

Rozendaal, M. A., C. B. Leovy, and S. A. Klein, 1995: An observational study of diurnal variations of marine stratiform cloud. *J. Climate,* **8,** 1795–1809.

Serpetzoglou, E., B. A. Albrecht, P. Kollias, and C. W. Fairall, 2008: Boundary layer, cloud, and drizzle variability in the southeast Pacific stratocumulus regime. *J. Climate,* **21,** 6191–6214.

Sharon, T. M., B. A. Albrecht, H. H. Jonsson, P. Minnis, M. M. Khaiyer, T. M. van Reken, J. Seinfeld, and R. Flagan, 2006: Aerosols and cloud microphysical characteristics of rifts and gradients in maritime stratocumulus clouds. *J. Atmos. Sci.,* **63,** 983–997.

Slingo, A., 1990: Sensitivity of earth's radiation budget to changes in low clouds. *Nature,* **343,** 49–51.

——, K. I. Hodges, and G. J. Robinson, 2004: Simulation of the diurnal cycle in a climate model and its evaluation using data from METEOSAT 7. *Quart. J. Roy. Meteor. Soc.,* **130,** 1449–1467.

Slingo, J. M., 1980: A cloud parameterization scheme derived from GATE data for use with a numerical model. *Quart. J. Roy. Meteor. Soc.,* **106,** 747–770.

Stevens, B., and Coauthors, 2003: Dynamics and Chemistry of Marine Stratocumulus—DYCOMS-II. *Bull. Amer. Meteor. Soc.,* **84,** 579–593.

Stull, R. B., 1988: *An Introduction to Boundary Layer Meteorology*. Kluwer Academic, 666 pp.

Wang, J., W. B. Rossow, T. Uttal, and M. Rozendaal, 1999: Variability of cloud vertical structure during ASTEX observed from combination of rawinsonde, radar, ceilometer and satellite. *Mon. Wea. Rev.,* **127,** 2484–2502.

Wittenberg, A. T., A. Rosati, N. C. Lau, and J. J. Ploshay, 2006: GFDL's CM2 global coupled climate models. Part III: Tropical Pacific climate and ENSO. *J. Climate,* **19,** 698–722.

Wood, R., and C. S. Bretherton, 2006: On the relationship between stratiform low cloud cover and lower tropospheric stability. *J. Climate,* **19,** 6425–6432.

Wylie, D., D. L. Jackson, W. P. Menzel, and J. J. Bates, 2005: Trends in global cloud cover in two decades of HIRS observations. *J. Climate,* **18,** 3021–3031.

Xu, H., S. Xie, and Y. Wang, 2005: Subseasonal variability of the southeast Pacific stratus cloud deck. *J. Climate,* **18,** 131–142.

Yuter, S. E., Y. L. Sierra, and R. A. Houze Jr., 2000: The 1997 Pan American Climate Studies Tropical Eastern Pacific Process Study. Part II: Stratocumulus region. *Bull. Amer. Meteor. Soc.,* **81,** 483–490.